Revealing Cellular Structures by Expansion Microscopy

Quantitative Expansion Microscopy on Synaptonemal Complexes in Mouse Spermatocytes

Maarten Slik

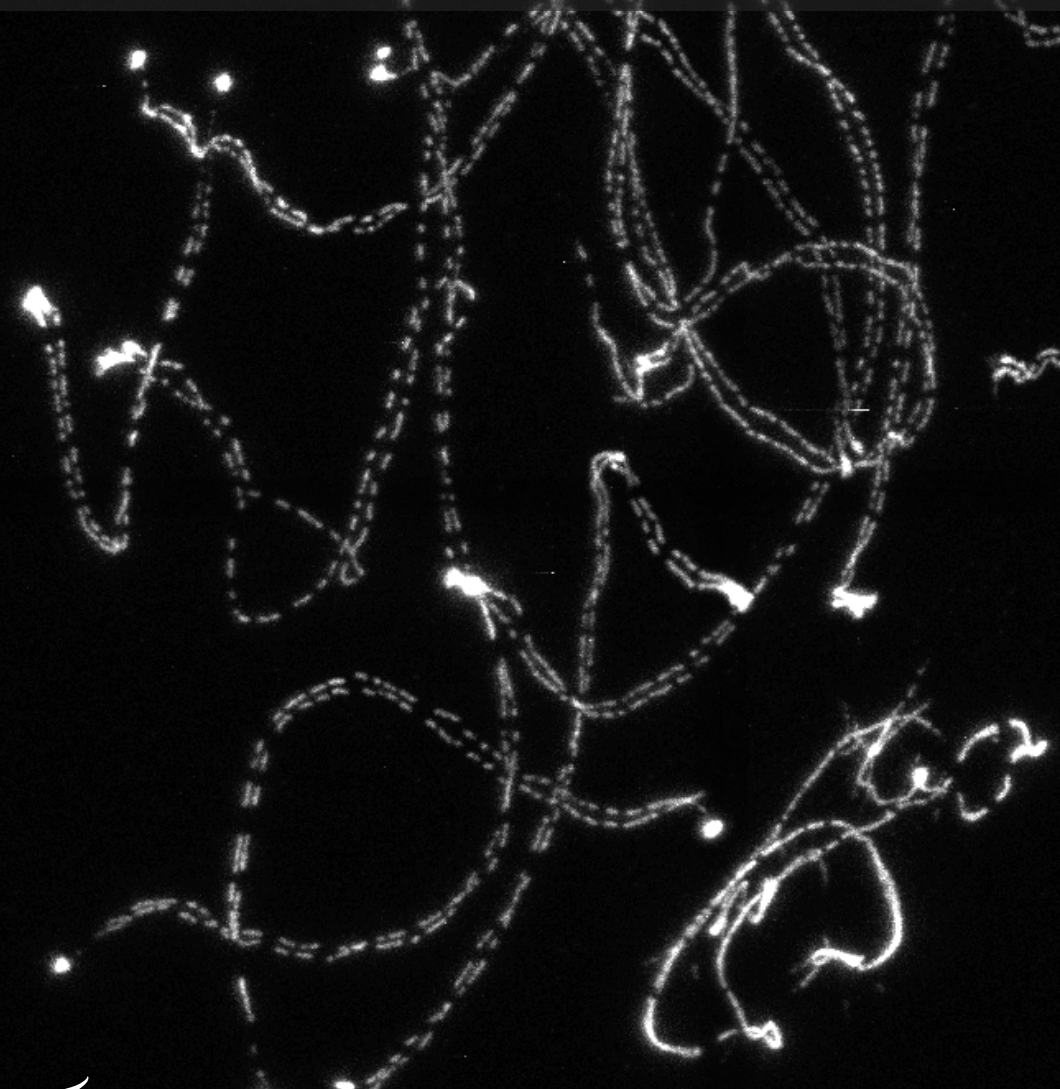

Delft University of Technology & Erasmus University Rotterdam

TU Delft

Erasmus MC
Universitair Medisch Centrum Rotterdam

Revealing Cellular Structures by Expansion Microscopy

Quantitative Expansion Microscopy on Synaptonemal Complexes in Mouse Spermatocytes

by

Maarten Slik

Student Name	Student Number
Maarten Slik	4833430

Instructor:	J.A. Slotman
First Examiner:	W.A. van Capellen
Second Examiner:	W.M. Baarends
Project Duration:	September, 2022 - February, 2023
Department:	Optical Imaging Centre

Cover: ExM on SYCP3 stained mouse spermatocytes

TU Delft

Preface

The work presented in this report feels like the culmination of my bachelor studies as a nanobiology student. This is a bittersweet moment as I am happy having finished my bachelor thesis, but saddened by the fact I still have many ideas on experiments for expansion microscopy which I can no longer carry out. I started my studies as a double bachelor student in Applied Physics and Mathematics. I did not choose nanobiology at first, because I feared that this study would not offer the technical foundation I desired. During my first year as a double bachelor student I discovered that I missed biology, which made me switch to nanobiology. I enjoyed working on this topic a lot, as this project offered me the typical interdisciplinary research which made me choose nanobiology in the second place. Therefore, I would like to thank Johan Slotman and Gert van Capellen for allowing me to do my bachelor end project at the Optical Imaging Centre of the Erasmus Medical Centre. Furthermore I would like to thank the rest of the OIC-team for their support and help during my time there. I would like to mention Tsion Abraham specifically as she guided me with experiments and showed me the way around the lab. My gratitude also goes out to Aditya Mhaskar at the Department of Developmental Biology of the Erasmus Medical Centre for his support.

Maarten Slik
Delft, February 2023

Contents

1

Introduction

Correct chromosome separation is crucial to proper gamete generation and creating viable offspring consequently. Spermatocytes pair homologous chromosomes during meiosis. An important part in meiosis is genetic recombination of homologous chromosomes during cross-over. To ensure interaction strictly between their homologous chromosomes, the SC (Synaptonemal Complex) functions as a scaffold backbone to which the homologous chromosomes are attached.

The SC is a cellular structure comprised of multiple substructures, each made of proteins. The substructures of the SC are the TF (transverse filament) , LE (lateral element), and a CE (central element) as shown schematically in figure 1.1. The TFs connect the homologous chromosomes, while the LEs holds the homologous chromosomes together and the CE connect the TFs in the middle of the SC. In this research the SYCP3 (Synaptonemal Complex Protein 3) is further investigated. SYCP3 is a protein important to the structure of the LE. Earlier research has shown that the distance between the LEs is approximately 100nm [9].

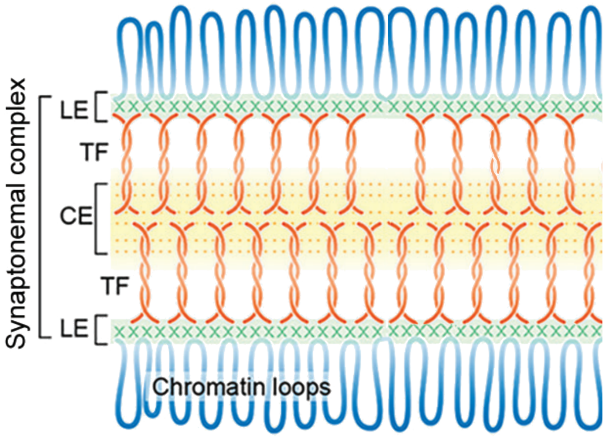

Figure 1.1: Complete schematic overview of the SC structure. In blue chromatin loops are shown, this is connected to the LEs (green) which are connected to the CE (yellow) through the TFs (orange). This image was adapted from [8].

The SC assembles and disassembles during meiotic prophase, which can be subdivided in five different stages. leptotene, zygotene, pachytene, diplotene, and diakinesis as seen in figure 1.2. During leptotene, the replicated sister chromatids are held together by cohesin complexes. LEs will start to build on the chromosomes. During zygotene, the homologous chromosomes are more closely and stably paired, this is called synapsis. This is achieved by the start of building the CE and TF of the SC. In zygotene stage, the LEs of the SC will have assembled between the chromosomes. Meitotic recombination is triggered by programmed DSB (double strand break) formation. In pachytene, homologous recombination, including chromosomal crossover, is completed through the repair of the formed DSBs. The SC will assemble completely along the entirety of the chromosome pair. Some of the breaks form

crossovers, resulting in the exchange of genetic information. Sex chromosomes will only exchange genetic information over the region where they share homology; the pseudo-autosomal region. During the diplotene stage, the SC will desynapse and chromosomes separate a little. The chromosome pairs remain constrained at chiasmata, regions where crossing-over events happened. This allows the chromosome pairs to move in to the opposite sides of in the cell. In the last stage, diakinesis, chromosomes will further remodel to become more condensed [8] [7].

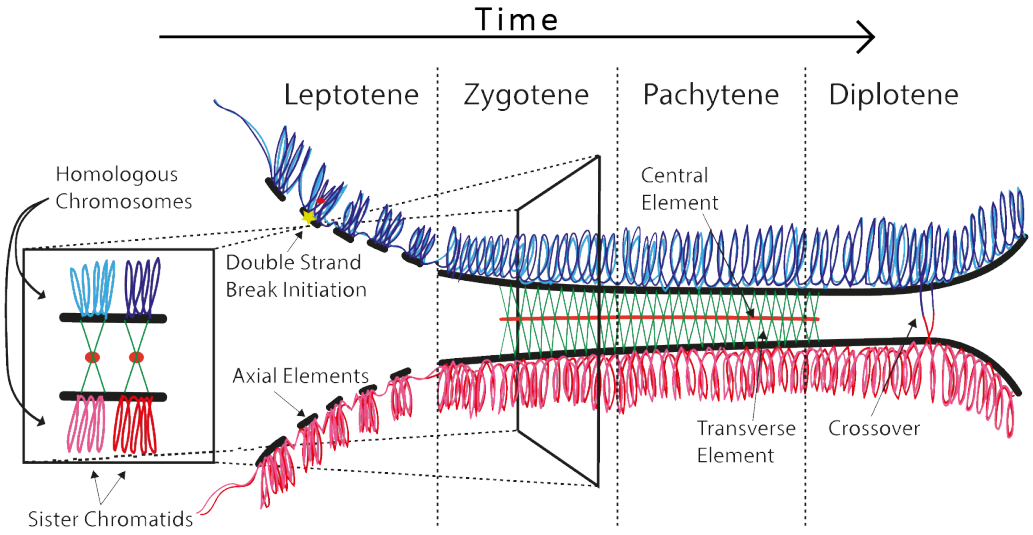

Figure 1.2: Schematic overview of the SC and chromosome structure with respect to the substages of meiotic prophase. The stages from left to right are leptotene, zygotene, pachytene, and diplotene, the order in which they occur chronologically. This image was adapted from [21].

Due to the scale of the SC and the inherent diffraction properties of light [4], resolving the LEs is impossible with an ordinary confocal microscope which is limited to a resolution of $\pm$250nm. 3D SC structure and function have been investigated thoroughly using super resolution microscopy [12], [13], [19] or electron microscopy [3]. Pitfalls of these techniques lie in expensive instruments and laborious sample preparation. Furthermore, all currently published research on SC structure is done with spread preparations. Although this work may not be dismissed, to justly bring the SC structure to light, it needs to be examined in a native state. Expansion microscopy (ExM) addresses these two problems. Using ExM biological material can be expanded in all three dimensions from 4 to 16 times [14] inside a swellable hydrogel. Additionally, ExM has been proven useful in combination with super resolution techniques [12] to go beyond the resolution of super resolution microscopy. Not just cultured cells, but also tissue samples have been expanded successfully with ExM [14].

1.1. ExM Principle

The main principle of ExM relies on fixating biological material and embedding this in a swellable hydrogel polymer network. A mix of acrylamide and sodium acrylate is most commonly used. After polymerisation, sodium acrylate becomes super absorbant and can hold its weight 100-1000 times in water [17]. This makes it an excellent choice for ExM. Through digestion or denaturing the biological material is relieved from its original structure. Without this structure, the hydrogel with the embedded material is hypothesised to expand isotropically [10], [14] in water.

ExM can serve as a useful tool extending the capabilities of a regular fluorescence microscope. While it does not increase resolution, through expansion the relative resolution is enhanced. Due to expansion, the protein dense interior of the cell is diluted. This opens up the possibility for fluorescent dyes or antibodies used in labelling to reach targets which would be sterically hindered before expansion. Due to dilution of the biological material, the final samples are comprised mostly of water and nearly free of aberrations. Because the biological material needs to be fixated in a hydrogel polymer network, ExM can not be in used live-cell analysis. Another downside to ExM is that handling hydrogels can be difficult rough and requires much practice. Lastly, cells can be lifted into the hydrogel after expansion. To solve this issue, costly long distance working objectives or cryosectioning of the sample

[9] may be needed to image an expanded cell fully.

In this research we are interested in the SC structure, which will be examined with an ExM protocol adapted from [14]. Before applying the protocol to mouse spermatocytes, U-2OS cells were used in order to conserve mice, and extensively test different conditions for expansion and staining. It is interesting to note that many varieties of ExM exist. There is no single best method. Earlier studies used proteases to digest the cellular structure which prevents isotropic expansion. The downside is that most cellular content is broken down in this way. Later studies have shown that cellular content can be expanded freely by denaturation of the cellular protein [14]. A mix of both digestion and denaturation is has been used as well [5].

1.2. Theory of Methodology

In this research the pan-ExM protocol from [14] was used. In the pan-ExM protocol a NHS-ester (N-hydroxysuccinimide) dye is used to stain all protein in their ultra-structural context . NHS is an amine-reactive reagent which can form a stable amide bond with compounds containing amino groups (which can be found in excess on proteins). The amino group needs to be unprotonated for the reaction to occur, which can be achieved with higher pH [1]. If the pH is too high, the NHS-ester can also react with hydroxy-ions or -groups [15] making the NHS-ester dye no longer reactive and unable to bond to amino groups on target proteins. Buffering the solution at pH=8.3 optimally accounts for these conflicting concerns [1].

The pan-ExM methodology consists of the following steps. The biological material or protein is treated with a solution of formaldehyde and acrylamide. Formaldehyde prevents inter-protein crosslinks and can covalently bond to the acrylamide monomer which will form the hydrogel polymer network during polymerisation. This will eventually link the hydrogel polymer network to the abundant free primary amine groups of proteins.

The protein will be embedded in three different hydrogels. A primary gel for a first round of expansion. A neutral hydrogel which will maintain the expanded structure during consequent processing steps. Lastly, a secondary hydrogel is made for a second expansion. The first hydrogel and neutral hydrogel are made with a cleavable cross-linker DHEBA (N,N′-(1,2-dihydroxyethylene)bisacrylamide). The sample is denatured and delipidated with SDS (sodium dodecyl sulfate) at 73°C. After expansion, the sample will have expanded around 4-fold in all dimensions. By embedding the expanded gels in the secondary hydrogel with a non-cleavable cross-linker, the primary and neutral hydrogel can be dissolved using a NaOH solution and washed away. The hydrogel will be expanded a second time (approximately 4-fold in all dimensions) when it will reach a final expansion of approximately 16-fold in all dimensions.

1.3. Expansion Factor

In order to relate images from expanded cells back to the original scales of cellular structures an expansion factor Q must be determined. Q is a dimensionless number which tells us the ratio to which a hydrogel has expanded in a single dimension. When areas or volumes are measured expansion should be accounted for in all dimensions. Q can be used to determine the original size of measured cellular structures via equation 1.1-1.3, when expansion is isotropic. When expansion is non-isotropic the different values for Q_x, Q_y, and Q_z with respect to the dimensions in which measurement takes place.

$$D_{original} = \frac{D_{expanded}}{Q} \tag{1.1}$$

$$A_{original} = \frac{A_{expanded}}{Q^2} \tag{1.2}$$

$$V_{original} = \frac{V_{expanded}}{Q^3} \tag{1.3}$$

Studies have determined Q (expansion factor) based on registration techniques with images acquired pre- and post-expansion [9], [12]. Other studies determined Q based on size comparisons of well-documented cellular structures [10], [14]. Retrieving the same cell post-expansion can be very hard

as hydrogels might break during expansion. In this research we looked into a stochastic determination of Q, allowing quantitative ExM. We hypothesised that fluorescent beads could be used to determine Q by imaging a set number of beads pre- and post-expansion with a tile scan. The distribution of the NN (nearest neighbour) length of the beads can be compared pre- and post-expansion. With this method the NN distribution in x, y, and z can be compared independently and possible inhomogeneities in expansion can be corrected for. Another way to determine expansion would be by comparing the imaged volumes, Q can be determined using equation 1.4. With this method, the assumption of complete isotropic expansion is made.

$$Q = \sqrt[3]{\frac{N_{beads,pre-ex} \cdot V_{post-ex}}{N_{beads,post-ex} \cdot V_{pre-ex}}} \tag{1.4}$$

Using avidin coated fluorescent beads, the beads could be subjected to the same post-fixation step as the protein from the biological material as described in section 2.5. This will hypothetically embed the beads in the hydrogel polymer network similarly to the biological material as avidin will have copious free primary amines.

A computer model simulating beads in a hydrogel was constructed. With this model the beads could undergo various transformations compared to normal hydrogel swelling. A numerical analysis was executed to determine which method is best fit to determine the expansion factor and establish a sample size of N_{beads} at which realistic values for Q can be determined.

1.4. Hydrogel Dynamics

It is important to understand the mechanics that come into play during hydrogel swelling. In figure 1.3 the molecular structure of the monomers that build the hydrogel polymer are shown. Water absorbance properties can be dedicated to both monomers. Firstly, sodium acrylate in a polymer network will have negative charges bound to polymer network and free positive charges dissolved in the polymer network [17]. When in contact with water, the free sodium will distribute equally between the hydrogel polymer network and the water. The sodium charges will be replaced by water through osmosis. The hydrogel will expand until the sodium concentration is between the water and hydrogel is balanced. Secondly, the free amine group of the acrylamide monomer can form strong hydrogen bonds with water molecules. This contributes to hydrogel swelling as well.

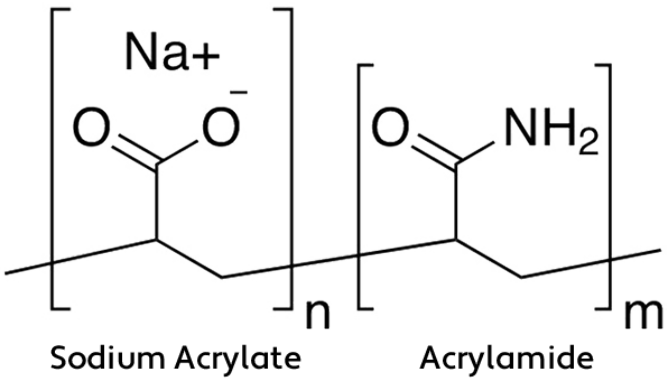

Figure 1.3: Molecular structure of the acrylamide-sodium acrylate polymer. The left monomer shown is the molecular structure of sodium acrylate, the right monomer shows acrylamide. Image adapted from [18]

2

Materials and Methods

2.1. Maintaining U-2OS Cell culture

Cells were cultured in Dulbecco's Modified Eagle Medium (DMEM, Gibco, REF. 21053-208) with 5% Fetal Bovine Serum (FBS, Gibco, REF. 10270-106), 1% L-Glutamine (Lonza, CAT. BE17-605E), 1% Penicillin-Streptomycin (Pen/Strep, Lonza, CAT. DE17-602E). Cells were cultured in a T75 culturing flask (Sarstedt, REF. 83.3911) and passaged when 90-100% confluency was reached. The cells were used from passages 7 until 25. Passaging was performed by washing twice with 1x Dulbecco's Phosphate Buffered Saline (DPBS (1x), Gibco, REF. 14190-094). Next, the cells were tripsinized with 1mL Trypsin-Versene Mixture (TVM, Lonza, CAT. 17-161E) and diluted according to confluency.

The cells were seeded on 18x18mm square cover slips (No. 1.5 H) in a six-wells plate. The cells were incubated at 37°C with 5% CO_2 until 70-80% confluency was reached.

2.2. Mouse Spermatocyte Harvesting

The spermatocytes were fixated on 24mm round cover slips. Firstly, the cover slip is cooked in water for 20 minutes in a microwave and dried overnight. The slips were coated in 100mL 0.01% poly-L lysine (Sigma-Aldrich, CAT. P8920) for 5 minutes and dried at 63°C.

Testis were removed from 17-18 days old euthanized mice. The testis were disrupted with a scalpel and 1x PBS and collected in a tube. The cell suspension was centrifuged at 9000rpm and re-suspended in 200µL 1x PBS. 10µL of cell suspension with 50µL 1x PBS was placed on while not covering it fully. After 15 minutes, the entire slide was covered with 4% paraformaldehyde (PFA, Electron Microscopy Sciences, CAT. 15710) in 1x PBS for fixation. The PFA was washed away with 1x PBS three times for 1 minute. The slides were dried for 1 hour and stored at -80°C for up to 3 months.

2.3. Cell fixation

U-2OS cells were washed once with 1x PBS and fixed with 3% formaldehyde (FA, Merck, CAT. 1.03999.1000) in 1x PBS for 15 minutes at room temperature. Spermatocytes and U-2OS cells were incubated in 1mL post-fixation solution (0.7% formaldehyde + 1% Acrylamide (AAm, Sigma-Aldrich, CAT. 1.10784.0100) in 1x PBS) for 6-7h at 37°C. U-2OS cover slips were washed twice with 1x PBS for 20 minutes on an orbital shaker, spermatocytes were washed on a rocking shaker.

2.4. Hydrogel Reagents

Sodium acrylate (SA; Chem Cruz, CAT. sc-236893), acrylamide (AAm; Sigma-Aldrich, CAT. 1.10784.0100), N,N'-Methylenebisacrylamide (BIS; Thermo Scientific, CAT. J66710), N,N'-(1,2-dihydroxyethylene)-bisacrylamide (DHEBA; Sigma-Aldrich, CAT. 294381), ammonium persulfate (APS; Fisher BioReagents, CAT. BP 179-100), N,N,N',N'-tetramethylethylenediamine (TEMED; Sigma-Aldrich, CAT. 87687), Sodium dodecyl sulfate (SDS; Sigma-Aldrich, CAT. 7172).

2.5. Fluorescent Beads in Primary Hydrogel

125µL Avidin yellow coated fluorescent polystyrene particles (G. Kisker, CAT. PC-AFY-0.5) were centrifuged at 18000rpm for 4 minutes and resuspended in post-fixation solution by vortexing until the pellet was no longer distinguishable. The post-fixation solution with beads was sonicated for 4 minutes. Next, the solution was post-fixated as described in section 2.3. After fixation the beads were centrifuged a second time at 18000rpm for 4 min. The beads were resuspended in 1x PBS by vortexing until the pellet was no longer distinguishable, after which a the solution was sonicated 4 minutes. The bead solution could be stored in the fridge up to 4 weeks, kept in a dark eppendorf tube.

When needed, the beads could be retrieved from storage by centrifuging as previously mentioned. Resuspend the beads in 1X PBS, SA, and AAm according to the primary hydrogel concentrations by vortexing until the pellet is no longer visible. Sonicate for 4 minutes. Add the rest of the primary hydrogel reagents.

2.6. Primary Hydrogel Gelation

A gelation chamber was constructed with siliconized glass slides [2] as base, scotch tape with a thickness of 64 ± 6µm as spacer, on top of which the glass slide with seeded cells were placed face down as seen in figure 2.1. This leaves a gap on both sides where the primary hydrogel solution (19% SA, 10% AAm, 0.1% DHEBA, 0.25% APS, 0.25% TEMED in 1x PBS + fluorescent beads) can be added with a pipette. After resting 15 minutes at room temperature, the gelation chamber was placed in a humidified incubator for 1.5h at 37°C.

Figure 2.1: Schematic of the gelation chamber. The glass slide is shown in grey, the silicon coating in green, the scotch tape spacer in dark grey, the glass slide in light blue and the cells in red.

2.7. Denaturation

Denaturation buffer composition and temperature were optimised for each sample. The principle remained the same where the cover slip with the hydrogel was removed from the gelation chamber and placed in a 6 wells plate. The gel was incubated in 1mL of (preheated) denaturation buffer, see table 2.1 for 15 minutes. The gel was transferred from the cover slip to an eppendorf tube with 1mL of (preheated) denaturation buffer. The tube was placed in a water bath or heating block for 1h or 2h. U-2OS cells were always denatured at 73°C in a water bath. Mouse spermatocytes were either denatured in the water bath at 73°C or in the heating block at 95°C with preheated buffer. After denaturing, the gels were washed 3x in 1x PBS for 30 minutes.

Table 2.1: Overview of the varieties of buffers and times used in denaturation. The buffer solutions were made in MilliQ water.

	SDS [mM]	NaCl [mM]	Tris [mM]	Time [h]
Standard	200	200	50	2
+Time	200	200	50	1
+NaCl	200	600	50	1
+Time+NaCl	200	600	50	2

2.8. First Expansion

The gel was placed in a culturing plate and submerged in MilliQ water. The MilliQ water was refreshed every 30 minutes three times, after which it was left overnight. The resistivity of the MilliQ water used was 18.2MΩ·cm.

2.9. Neutral Gel Embedding

The expanded hydrogels were punched into 1x1cm pieces and re-embedded 3 times in 1mL neutral hydrogel solution (10% AAm + 0.05% DHEBA + 0.05% APS + 0.05% TEMED in 1x PBS) for 20 minutes on an orbital shaker at RT. The hydrogels were sandwiched between two 18x18mm cover slips making sure to remove excess gel solution with a tissue. The cover slips were weighted down lightly to keep them flat, after which they were incubated in a humidified chamber for 1.5h at 37°C. After polymerisation, the gels were washed 3x with 1x PBS in a six-wells plate for 30 minutes on an orbital shaker.

2.10. Post Fixation

Gels were incubated in post-fix solution (0.7% FA + 1% AAm in 1× PBS) for 15 minutes at room temperature and then for 6–9h at 37°C. The gels were subsequently washed 3x with 1× PBS for 30 minutes each on an orbital shaker at room temperature.

2.11. Secondary Hydrogel Embedding

The hydrogels were embedded 4x in 1mL secondary hydrogel solution (19% SA + 10% AAm + O.1% BIS + 0.05% APS + 0.05% TEMED in 1x PBS) in a 12 wells plate placed on ice for 15 minutes on an orbital shaker. After secondary hydrogel embedding, the gels were sandwiched between two 18x18mm cover slips. Residual hydrogel solution was removed carefully with a tissue. The cover slip hydrogel sandwich was placed in a humidified chamber for 2h at 37°C.

To remove the previous polymer networks the DHEBA cross linker is dissolved using a 0.2M NaOH solution. The gels were incubated in 1mL of 0.2M NaOH for 1h on an orbital shaker at room temperature. Afterwards, the gels were washed 3x with 1x PBS on an orbital shaker at room temperature.

2.12. Staining

For pan-staining two stock solutions of 20g/L NHS ester-ATTO594 (Sigma-Aldrich, CAT. 08741), NHS ester-ATTO488 (Sigma-Aldrich, CAT. 41698) in dimethyl sulfoxide (DMSO, Honeywell, CAT. 34869-1L) were made. The NHS ester dyes were diluted 1:1000 in a 100mM sodium bicarbonate solution. A 1g/L Hoechst stock solution was used and diluted 1:600 in a 100mM sodium bicarbonate solution. The NHS ester and Hoechst dyes can be diluted in the same solution. For PI (propidium iodide) staining, a stock solution of 5g/L was used and diluted 1:400 in MilliQ. For the respective dyes, the gels were incubated in 350µL of staining solution and incubated for 1.5h on an orbital shaker at room temperature. The gels were washed 3x with 1x PBS for 20 minutes on an orbital shaker.

For SYCP3 staining mouse anti-SYCP3 (Abcam, CAT. ab97672) primary antibody and goat anti-mouse-555 (Invitrogen, CAT. A21422) secondary antibody were used. The gels were washed once with 1 mL PBST (0.1% (v/v) Tween-20 (VWR Chemicals, CAT. 663684B) in 1x PBS) and twice on an orbital shaker for 20 minutes. PBST was removed by washing 3x with 1mL PBS. Next, the gels were washed 3x with 1mL of blocking solution (PBS^+) (0.5g BSA (Roche Diagnostics, CAT. 10735094001) + 0.15g Glycin (Merck, CAT. 1.04201.1000) in 100mL 1x PBS), followed by incubation in PBS^+ for 1h on an orbital shaker at room temperature. The blocking solution was removed and the gel was incubated with 500µL primary antibody diluted 1:2000 in PBS^+ on an orbital shaker for 24h at room temperature. The gels were subsequently washed 3x with 1mL PBST, followed by 3x 20 minutes wash on an orbital shaker at room temperature. The gels were then incubated with 500µL secondary antibody diluted 1:1000 in PBS^+ on an orbital shaker for 24h at room temperature. Afterwards, the gels were washed 3x with 1mL PBST, followed by three 20 minute washes with PBST on an orbital shaker at room temperature. Lastly, any residual PBST was removed by washing 3x with 1mL PBS.

2.13. Secondary expansion

The gel was placed in a culturing plate and submerged in MilliQ water. The MilliQ water was refreshed every 30 minutes three times, after which it was left overnight. The resistivity of the MilliQ water used was 18.2MΩ·cm.

2.14. Image Acquisition

Confocal images were acquired using a Leica SP8 [6] equipped with a white light laser and 405 diode laser. All images were acquired using either a HC PL APO 20x/0.75 air objective, HC PL APO 40x/1.30 oil objective, HC PL APO 63x/1.40 oil objective, HC PL APO STED 86x/1.20 motCORR water objective, or a HC PL APO STED 100x/1.40 oil objective. Imaging parameters were set using Application Suite X software (LAS X; Leica Microsystems). Hoechst and PI dyes were imaged with 405nm excitation. ATTO594 was imaged with 591nm excitation. ATTO488 and avidin yellow beads were imaged with 488nm excitation. Goat anti-mouse-555 was imaged with 561 excitation. The emission light from the dyes was imaged using gated spectral GaAsP hybrid detectors with the emission filter set from ($\lambda_{excitation} + 10$) to ($\lambda_{excitation} + 60$).

2.15. Computational Analysis

Image stacks of fluorescent beads were used and analysed in ImageJ (computer code available in appendix A.1). With a maximum projection of the stack, the local maxima of image I were determined with $threshold = I_{avg} + I_{std}$ and measured to determine coordinates (x, y). The z-profile was taken at each coordinate and fitted with a gaussian function to determine the z-coordinate of the every bead. The data was further analysed in Python.

The computer model to simulate hydrogel swelling was built in Python (computer code available in appendix A.2). In this model Q (expansion factor) can be determined using the nearest neighbour method or via volume based comparison as described in section 1.3. The theoretical accuracy in Q was determined by averaging 100 iterations for a determination of Q with N_{beads_pre-ex} and $N_{beads\_post-ex}$ equal to the imaged beads pre- and post-expansion.

3

Results

In this chapter, the results of the complete experimental series will be presented. The chapter is subdivided in three sections, hydrogel expansion factor (section 3.1), U-2OS expansions (section 3.2), and spermatocyte expansions (section 3.3).

3.1. Hydrogel Expansion Factor

To determine Q, a substantial volume of the hydrogel with fluorescent beads was imaged with a z-stack tilescan. From a maximum projection, the xy-coordinates were determined by measuring the maxima thresholded at $threshold = I_{avg} + I_{std}$. The z position was determined by fitting a gaussian to the z-profile of each xy-coordinate. Knowing the 3D position of each bead in the volume, the NN distance was computed for every bead. All NN distances were reduced to their x, y, and z dimension to determine the NN_{mean} and NN_{std} of the one-dimensional distributions of NN distances. This method was checked with a computational model generating random points and scaling them in x, y, and z by 3, 20, and 5 respectively. This was done inhomogeneously in such extremes to check whether comparison of pre- and post-expansion NN distributions can verify anisotropic expansion. With this method $Q_x = 5.2$, $Q_y = 5.2$, and $Q_z = 5.7$ when the NN distributions of random pre- and post-scaling points were sampled. This tells us that by random sampling of pre- and post-expansion beads, the anisotropic expansion cannot be retrieved from the data. Every point has a different NN after anisotropic expansion. Therefore, comparison of NN distributions will not yield the original scaling factors. We discovered that only on comparison of the exact same points pre- and post-expansion, their NN distributions could be correlated to retrieve the original scaling in x, y, and z of 3, 20, and 5. Comparing the exact same beads is trivial in a computational model but left a challenge for real hydrogels.

To test whether real life comparison of imaged beads pre- and post-expansion is possible z-stack tilescans were made from hydrogels loaded with beads pre- and post-expansion. These z-stacks were reduced to a maximum projection and image registration programs from ImageJ were exhausted in an attempt at correct registration without success. Next, a maximum projection was duplicated and transformed through translation and rotation ($x + 300, y + 300, \phi = 30°$). Registration of this elementary transformation failed as well as shown in figure 3.1. In the figure 3.1AB we see many bright spots, but mostly dark background. Both images have low information density causing image registration algorithms to get 'stuck' in local minima when registering both images as seen in figure 3.1C. This tells us that recovering post-expansion beads to compare the NN distribution is impossible.

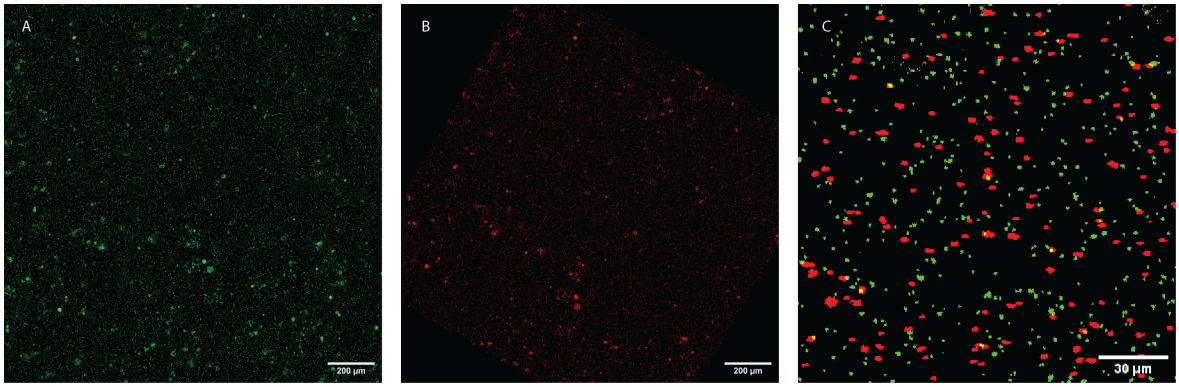

Figure 3.1: Example of failed registration of fluorescent beads in a hydrogel after translation and rotation $(x + 300, y + 300, \phi = 30°)$. A) Maximum projection of a z-stack of fluorescent beads. B) Maximum projection of z-stack of fluorescent beads after rigid transformation. C) Result of transformed image (yellow) registered on the original image (green) of fluorescent beads showing complete misalignment of beads.

Because image registration proved impossible, determination of Q was done with the second method proposed by 1.3 and equation 1.4. Random points were generated and scaled 4.6 times homogeneously in all dimensions. Accuracy was determined by randomly sampling $N_{beads,pre}$ and $N_{beads,post}$ in a range from 10^2 to 10^6 in computer simulations for 100 iterations. The standard deviation was calculated from the results of all iterations to determine accuracy of Q by equation1.4. The results are shown in figure 3.2. From the figure we see that when less beads are sampled, determination of Q becomes more inaccurate. It is important to note that determination of Q with this method assumes complete isotropic expansion of the hydrogel.

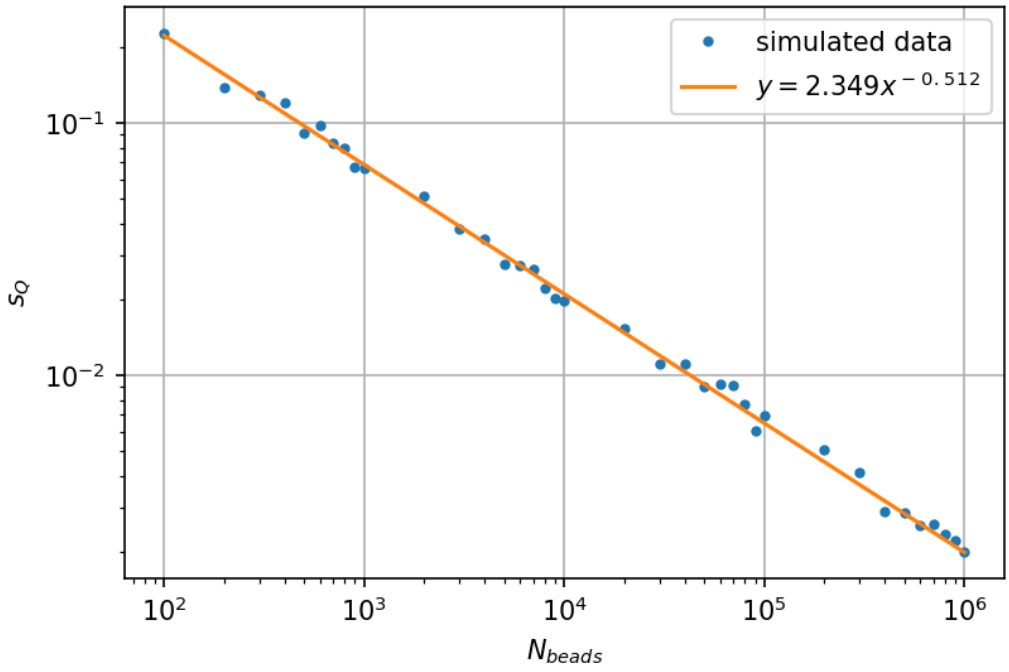

Figure 3.2: Logarithmic plot of the standard deviation in Q from all iterations against the number of beads sampled in the total volume. To the data an exponential is fitted in orange.

To gain more insight in hydrogel swelling and allow us to control expansion [22], multiple hydrogels were expanded in a saline series as shown in figure 3.3. Q was determined with equation 1.4 for all gels and plotted against the NaCl concentration, which is shown in figure 3.4.

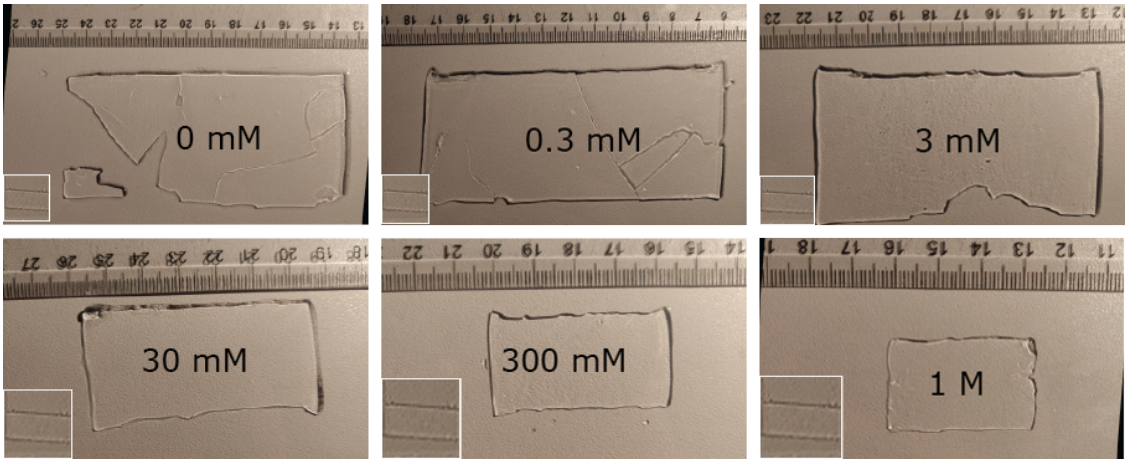

Figure 3.3: Overview of hydrogel expansion when swelling was done with different NaCl concentrations. In each image, a centimeter ruler and respective NaCl concentration is shown. From the image tears can be seen in the bigger gels. In each sub-image a non-expanded hydrogel of 18x8mm is displayed to scale

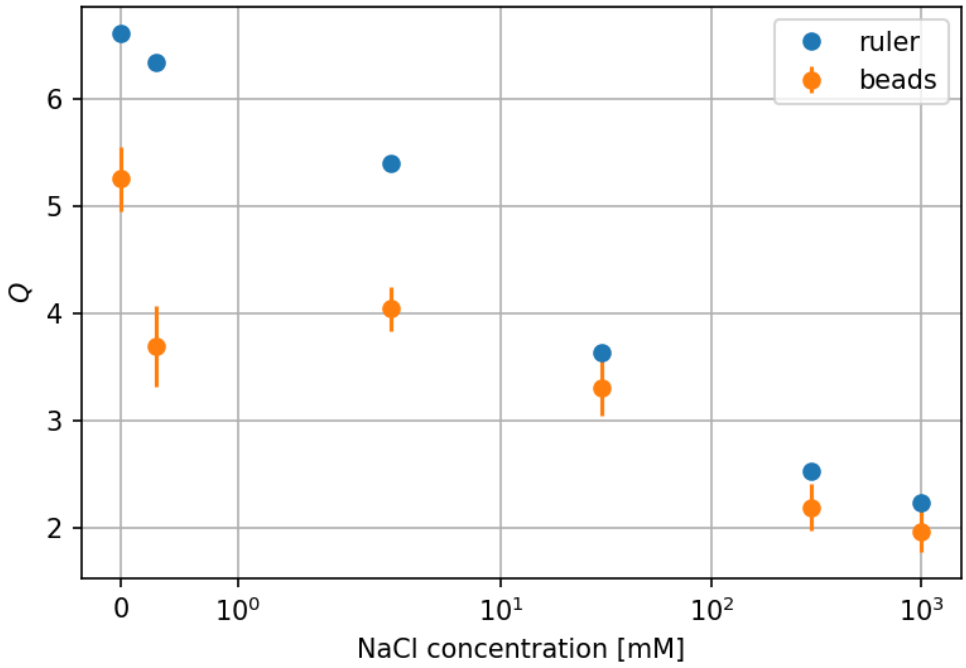

Figure 3.4: Expansion factor for single expansion plotted against NaCl concentration for the gels from figure 3.3. Measurements were done with a ruler or by comparing the volumes which hold equal N_{beads}. The errorbars are calculated with the fit from figure 3.2.

From the images we see that when salt concentration increases, hydrogel swelling decreases. This can be explained through the mechanisms described in section 1.4. This can be used to determine expansion rate roughly beforehand when maximum expansion a hydrogel can reach is not needed. Hydrogels remain more firm when expanded less, making which makes handling easier. As seen in figure 3.3 gels which have been expanded in lower NaCl concentrations have tears, gaps, or miss pieces which occured in handling hydrogels after expansion. On top of that, it can be seen that the width and length are not constant over the entire hydrogel, making ruler measurements inaccurate opposed to comparing sampled beads. In figure 3.4 it stands out that Q does not follow the same trend when Q is determined by ruler. This was caused by the hydrogel tearing in many places leaving less

material to image on the microscope, which increases the inaccuracy of Q as seen in figure 3.2

3.2. U-2OS Expansions

In this section, results of hydrogel expansion with U-2OS cells will be presented. These expansions were done to test the expansion conditions on biological materials we preformed expansion on U-2OS cells.

In figure 3.5 a comparison between a non-expanded cell and single expanded cells is shown. These cells were stained with Hoechst and NHS-Atto594. From the image we can see that after expansion, many details from the cellular structure are now are visible which are not distinguishable before expansion. For this expansion $Q = 3.89 \pm 0.038$. Multiple markers are added to show cellular structures which are not resolved in the non-expanded cells.

The scale bar length in 3.5BC C was chosen to reflect the similar length as the scale bar in 3.5A if the size of the expanded cell was related back to its original size using the expansion factor. The number depicted next to the scale bar is the actual size the cells have become after expanding. This allows us to easily relate back to the original size pre-expansion. This method is used for all following expansion images.

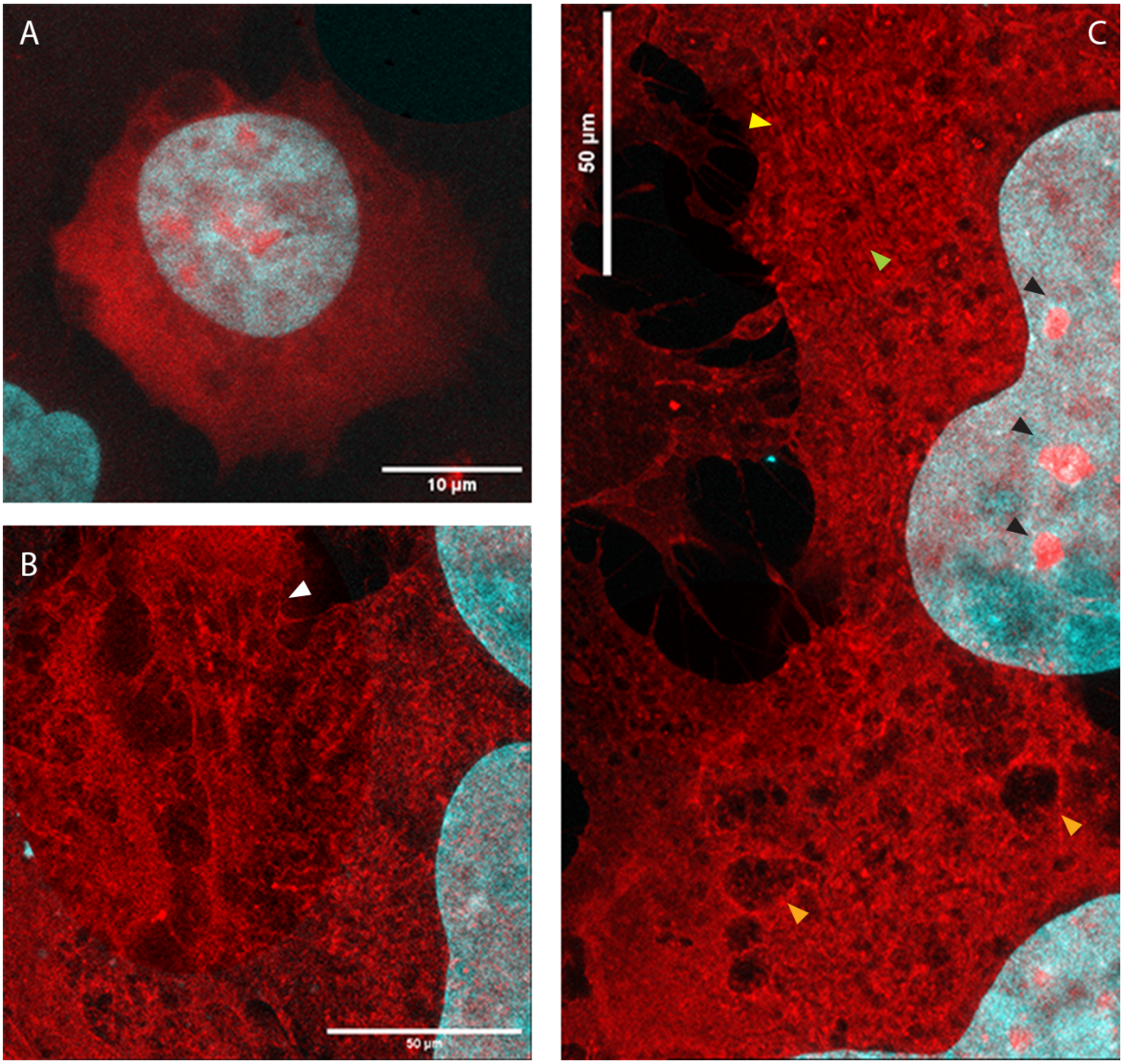

Figure 3.5: Single expansion on U-2OS cells, with $Q = 3.89 \pm 0.038$, stained with Hoechst (cyan) and NHS-Atto594 (red). A) maximum projection in Z of a normal cell. B) Z-slice from single expanded cell with a marker showing structures resembling focal adhesions. C) Z-slice from single expanded cells with markers indicating cellular structures resembling golgi apparatus (yellow), mitochondrium (green), and nucleoli (black). The included scale bars resemble the true size and are not corrected for expansion.

We can see much more detail in the cellular structure after expansion. The markers indicate structures which are not resolved in the pre-expansion cell. In both expanded and non expanded cells from image 3.5AC we can see protein dense regions inside the nucleus, which led us to believe they are nucleoli. By staining expanded U-2OS cells with propidium iodide to stain RNA and DNA we could test our hypothesis and compatibility with other dyes. The results of the PI staining are shown in figure 3.6. The result of the PI staining shows clear overlap of the signals from protein-dense regions in the cell nucleus stained by the NHS-ester dye and PI staining. It is interesting to note that it seems that much of the signal from PI staining is lost after expansion, because we see near overall overlap between the red and green signal in figure 3.6A. When denaturing the biological material pre-expansion, the sample is treated with SDS which might can wash away much of the cellular RNA.

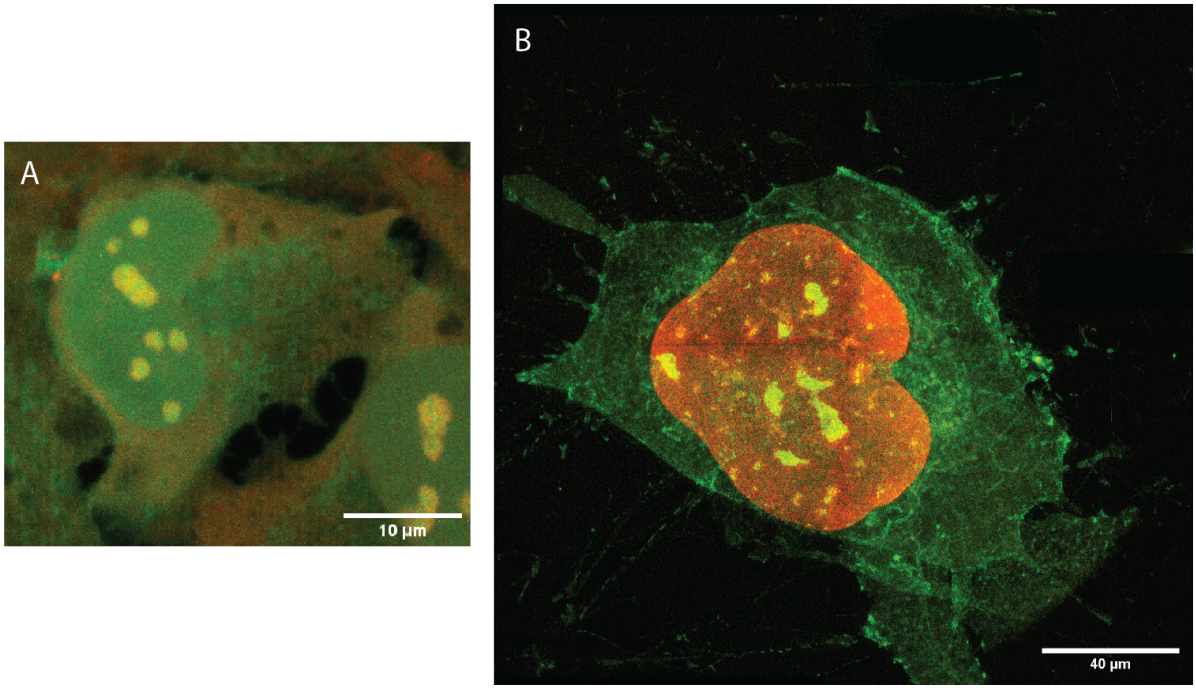

Figure 3.6: Comparison between a normal (A) and single expanded cell (B) stained with PI (red) and NHS-Atto488 (green). $Q = 3.8 \pm 0.012$, the scale bars resemble the true size and are not corrected for expansion. B was imaged with a tile scan, of which the lines can be seen in the image.

Next, cultured cells were were submitted to a second round of expansion as shown in figure 3.7. Double expansion resulted in $Q = 10.7 \pm 0.13$. Note that the error for this Q is higher than for single expansion because a similar value for N_{beads} will take exponentially longer due of expansion. Along the cell nucleus structures reminiscent of the endoplasmic reticulum can be seen, but this can not be said with certainty. This can be confirmed by staining the cultured cells with a counter stain [20] against ER, making sure not to select a dye with a far red emission spectrum as this will overlap with the emission spectrum of the NHS-Atto594 dye.

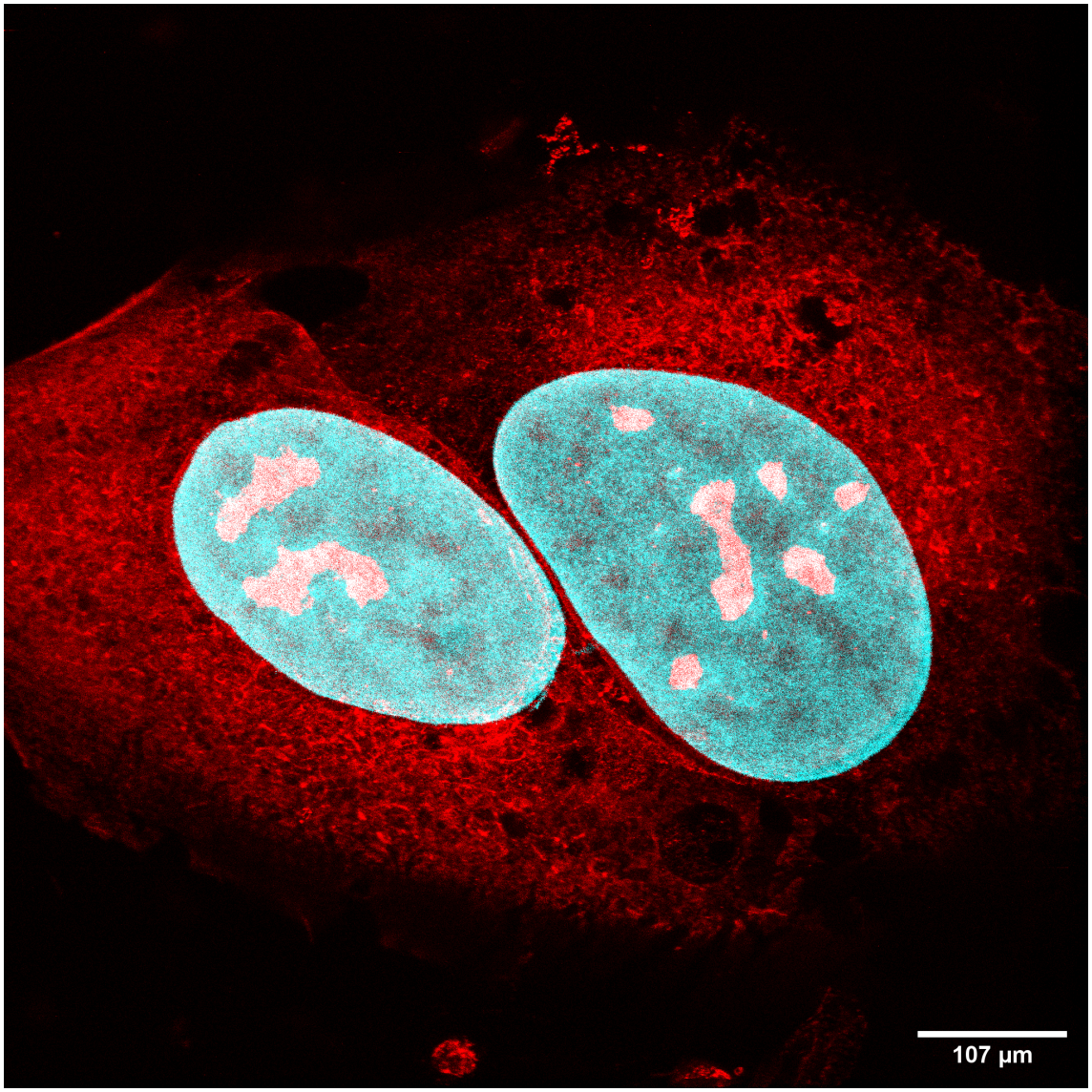

Figure 3.7: Confocal image of a U-2OS cell stained with Hoechst (cyan) and NHS-Atto594 (red) after double-expansion. For this expansion $Q = 10.7 \pm 0.31$.

We observe that pan-staining with NHS-ester dyes can give clear ultra-structural context within the cell. To confirm that the marked structures are indeed what they seem, counter staining (such as the PI staining in figure 3.6) against these organelles/structures must be done to to tell with certainty.

3.3. Spermatocyte Expansions

With knowledge, skills, and a clear method for determination of Q we moved on to mouse spermatocytes for quantitative ExM on the SC. We stained against SYCP3, a protein in the LE structure of the SC on isolated cells from mice. This is shown in figure 3.8A. Spermatocytes were stained pre-expansion, because we assumed that immunolabelling of SYCP3 would not work correctly after denaturing the spermatocytes. The isolated cells were embedded in a hydrogel and expanded once as shown in figure 3.8B. Comparing images with each other, the LEs are unresolved pre-expansion and not many details from the SC structure is seen. The latter image offers more detail about the SC structure. In figure 3.8B a yellow marker is placed where LEs are resolved. Furthermore rupture-like black spots (indicated with a white marker) along the SC are seen, which are not seen in the pre-expansion spermatocytes. We noticed that the hydrogel swells a little when initially placed in the denaturing buffer. This left us wondering if these ruptures are caused by incomplete denaturing or whether the SC tears when the

hydrogel swells initially due to the buffer when the proteins are not yet denatured.

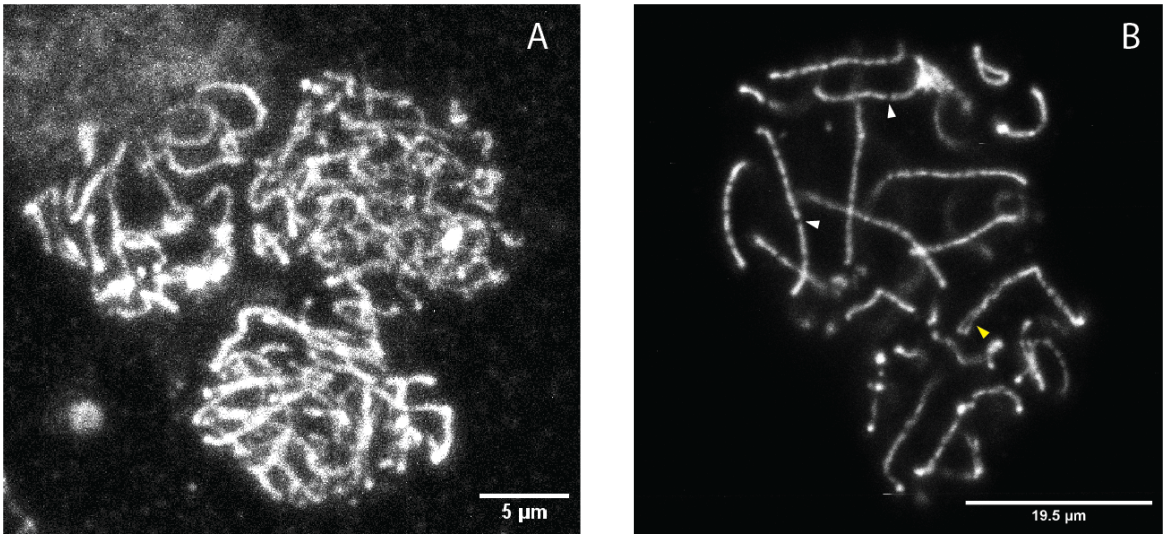

Figure 3.8: Confocal image of SYCP3 stained mouse spermatocytes before (A) and after expansion (B). A yellow marker is placed indicating a spot where the different axes of the SC can be resolved. A white marker is placed to indicate SC ruptures. $Q = 3.9 \pm 0.032$.

A multitude of denaturing tests were done, an overview can be found in table 2.1. To counteract initial swelling a denaturing buffer with increased NaCl concentration from 200mM to 600mM (based on the results in figure 3.4). To investigate if these ruptures are caused by incomplete protein denaturing, denaturing time was increased from 1h to 2h. A denaturing test with increased NaCl concentration and time was done to test the combined effect of both conditions. To check if more or less ruptures occured along the SC, the signal profile along the SC was analysed in ImageJ. The signal ratio (η) along the SC was used as a measure in determining if more or less ruptures occured in the SC. The results are shown in figure 3.9. For these denaturing tests, Q was not determined as this was not necessary for these series of tests.

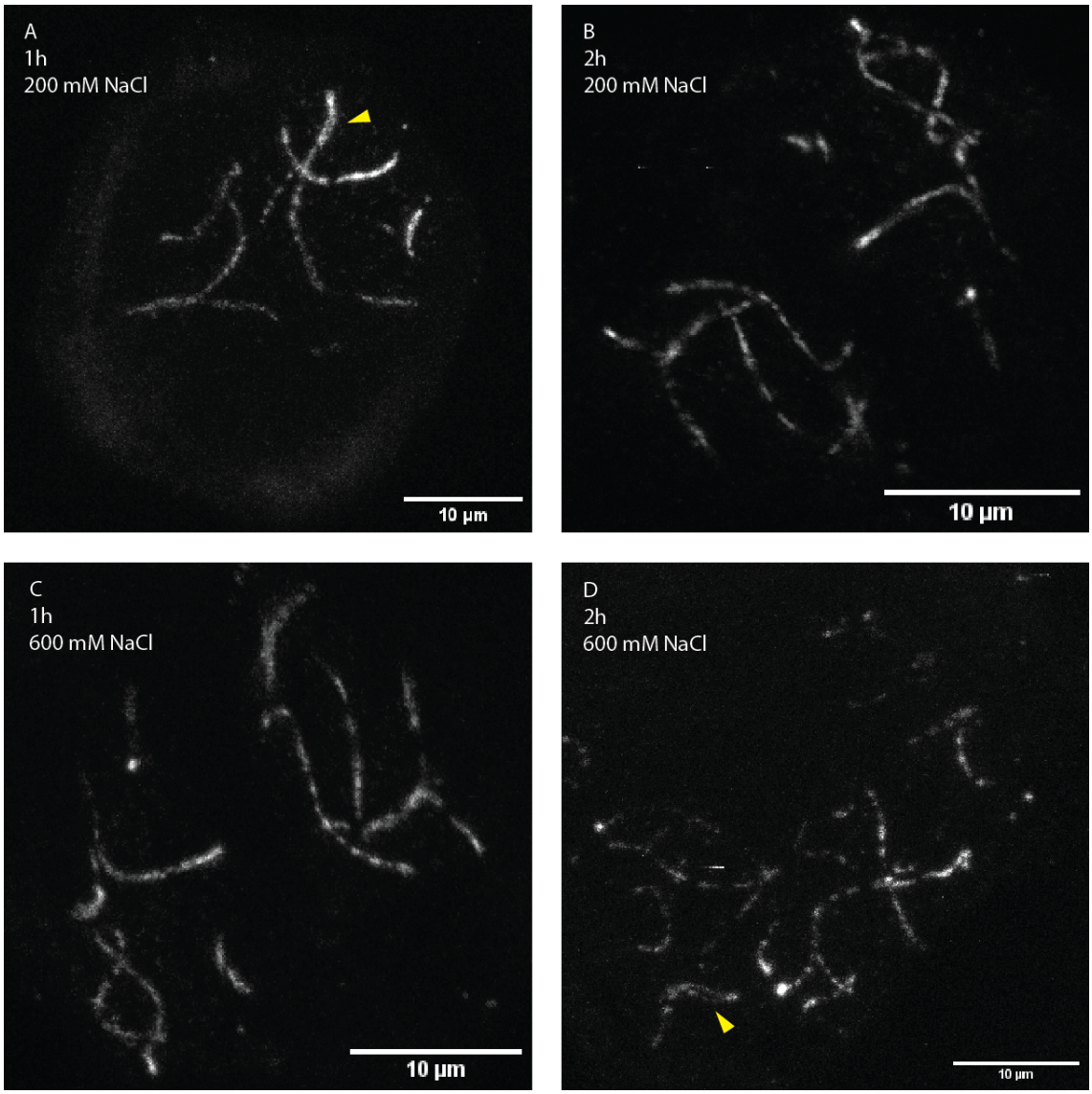

Figure 3.9: SYCP3 stained in mouse spermatocytes. A) Standard denaturing for 1h and 200mM NaCl B) Denaturing with increased time of 2h C) Denaturing for 1h with increased NaCl concentration to 600mM D) Denaturing for 2h with increased NaCl concentration to 600mM. Q was not determined for these results. Yellow markers indicate spots where both LEs are resolved.

Table 3.1: Mean percentages of signal (η) along the SC for all denaturing tests in the first column. The second column shows the standard deviation of η. The third column shows the number of cells analysed. The last two columns shows by which degree the parameters of denaturing are changed.

	η [%]	s_η	N	Time [h]	NaCl [mM]
Standard	66.1	6.2	6	1	200
+Time	61.7	11.3	3	2	200
+NaCl	73.9	14.8	3	1	600
+Time+NaCl	70.2	10.5	13	2	600

From the results in figure 3.9 and table 3.1 a slight positive effect on η is seen when the biological material is treated with a denaturing buffer with increased NaCl concentration. To tackle the problem of ruptures in the SC we looked into previous ExM publications on SYCP3. This is when we adapted the denaturing protocol from [9], which uses a similar standard buffer, 1h denaturing time, but increased denaturing temperature of $T = 95°$C and a preheated buffer. To our surprise, we found that immunola-

belling was done post-expansion. This allowed us to take advantage of decreased steric hinder in the protein dense pre-expansion cell, an important feat of ExM. Because immunostaining after expansion is more laborious, at first no beads were imaged so that the results of this new staining and denaturing could be analysed quickly.

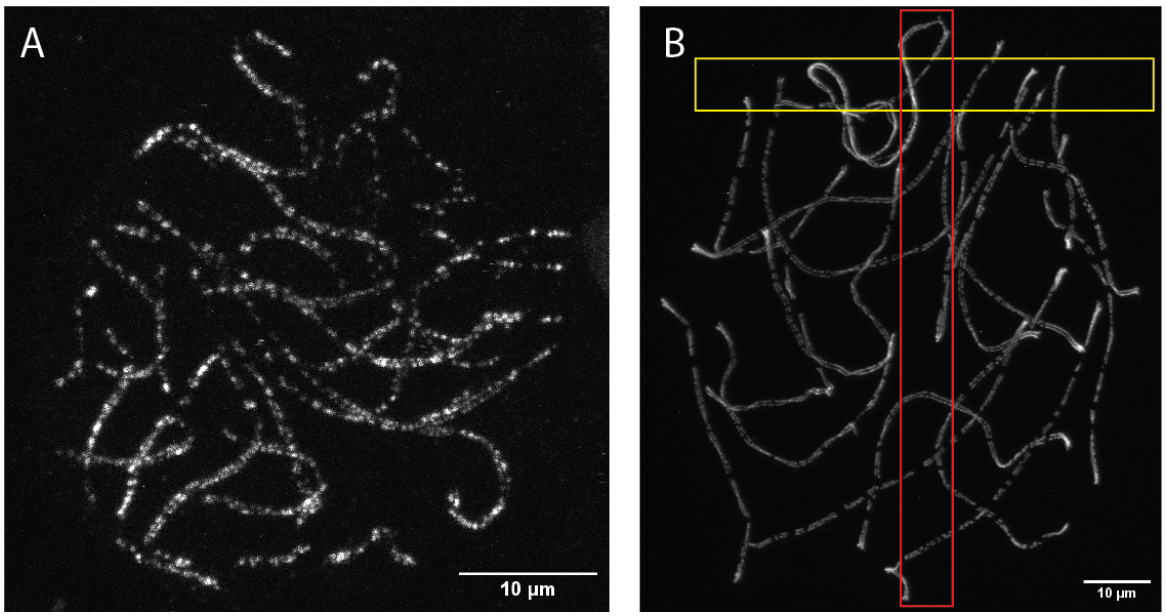

Figure 3.10: SYCP3 staining in mouse spermatocytes post-expansion with normal denaturation (A) and post-expansion staining with denaturation at 95°C (B). For these images, Q was not determined. A maximum projection of the resliced red and yellow domain is shown in figure 3.11.

Figure 3.10 shows the result of post-expansion staining (figure 3.10A) and post-expansion staining combined with increased denaturing temperature (figure 3.10B). Comparing post-expansion staining with pre-expansion staining the imaged LEs have more noise surrounding the SC axes and only few show resolved LE structures opposed to post-expansion staining where less noise surrounds the SC structures and the majority of SC structures have resolved LEs. Comparing SC signal ratios of post-expansion immunostaining with normal denaturing and denaturing at 95°C with a preheated buffer $\eta = 66.8 \pm 9.52$ (N=5) and $\eta = 84.4 \pm 5.8$ (N=5) respectively. Denaturing at 95°C with a preheated buffer increases signal ratio along the SC axis with 27%. This shows that denaturing at higher temperatures with a preheated buffer greatly increases the signal ratio along the SC axis and decreases ruptures in the SC structure. Expansion on mouse spermatocytes must be done in combination with denaturing at 95°C and increased NaCl concentration at 600 mM to test whether this can further increase signal ratio along the synaptonemal complex axis. On top of that, all SC axes show resolved LEs depending on the orientation of the SC in the cell. This begs the question if the LEs can be resolved axially as well, as the z-resolution of confocal microscopes is lower than the 100nm distance between the LEs. The image is resliced in ImageJ with a maximum projection in x and y shown in figure 3.11. No scale bars are included as voxel size information is lost when reslicing a z-stack in ImageJ. The top image shows that the SC structure can be resolved in complex configurations. The LEs of the SC structure are not resolved axially. Typical confocal microscopes have an axial resolution around 1 µm. With the distance between the LEs at 100nm and $Q \simeq 4$ it is not expected that the LEs can be resolved axially after single expansion. The best example is shown in the bottom image. Post-expansion immunostaining of SYCP3 should be further investigated with a double expansion which has the potential to resolve the LEs axially.

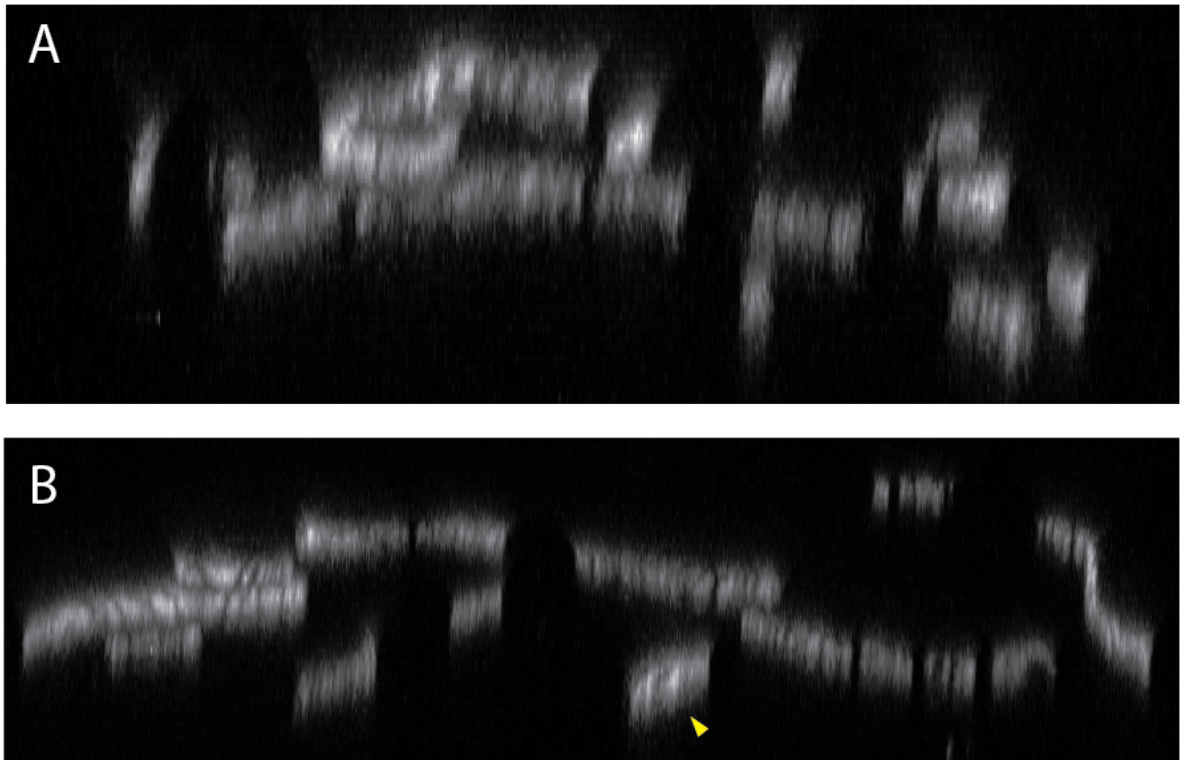

Figure 3.11: Figure 3.10B resliced in the x and y dimension (figure A and B respectively). (A) Max projection of the resliced yellow domain in figure 3.10B. (B) Max projection of the resliced red domain in figure 3.10B. Marker placed to show where LEs are nearly resolved axially.

4

Discussion

We set out to to investigate SC structure in mouse spermatocytes in a native state using quantitative ExM. In this research we found that fluorescent beads can be used to quantitatively determine expansion factor, Q, in two ways. The first method is correlating the nearest neighbour (NN) distribution of the pre- and post-expansion beads, if the same set of beads are correlated with each other. This proved nearly impossible as image registration algorithms are not able to register confocal images of such beads, because these algorithms will get stuck in local minima when optimising registration due to the low amount of information held in fluorescent bead images. For further research it might be interesting look into point-set registration techniques [16]. These algorithms might be the solution in registering post-expansion beads to pre-expansion beads. We did not look into this method due to time constraints. Therefore we used another method to quantitatively determine Q. The second method, in which beads were sampled pre- and post-expansion, uses equation 1.4 to determine Q quantitatively. With this method, complete isotropic expansion of the hydrogel is assumed. Using computer simulations, we were able to determine a theoretical error based on the number of beads sampled pre- and post-expansion plotted in figure 3.2.

With a quantitative determination of Q hydrogel swelling was investigated by submitting multiple hydrogels to a single expansion with a saline series. A NaCl concentration of 0, 0.3, 3, 30, 300, and 1000mM yielded $Q = 1.97 \pm 0.20$, $Q = 12.19 \pm 0.22$, $Q = 3.31 \pm 0.26$, $Q = 4.04 \pm 0.21$, $Q = 3.69 \pm 0.38$, $Q = 5.25 \pm 0.30$ respectively. This shows that salt concentration influences hydrogel swelling inversely and can be used to expand a biological sample to a desired size when maximum expansion is not desired.

The conditions of the pan-ExM protocol was tested on U-2OS cells to conserve mouse spermatocytes. These tests showed promising results with resolved cellular structures after a single expansion which are not resolved before expansion. After a double expansion more detail in the cellular structure can be seen, giving clear insights into the cellular ultra structure. This allows us to see proteins, structures, and organelles in their context, but counter staining must be done to elucidate what is seen exactly. When choosing a counter stain it is important to choose the dyes carefully to make sure that their emission spectra will not overlap. Luckily, NHS ester dyes can be conjugated with a plethora of dyes making choice in a wide range possible. We performed a propidium iodide staining to show compatibility with the pan-ExM protocol. This showed that the bright nuclear protein-dense regions gained through NHS-ester dye staining are in fact nucleoli.

Isolated mouse spermatocytes were subjected to single expansions and stained against SYCP3. Here we found that ruptures along the SC axis occured in post-expansion spermatocytes. We tried optimising denaturing by increasing denaturing time to 2h and salt concentration of the buffer to 600mM which did not reduce ruptures along the axis significantly. By increasing the denaturing temperature to 95°C in combination with preheating the buffer the signal ratio along the SC axis was increased by 27% from $\eta = 66.8 \pm 9.52$ to $\eta = 84.4 \pm 5.8$. Furthermore, we showed that staining of SYCP3 is possible after this more intense denaturing post-expansion. Images of post-expansion stained SYCP3 shows more details with nearly all LEs resolved depending on their orientation. Single expansion does not offer a big enough resolution increase in order to resolve LEs axially. Double expansion can theoretically resolve the LEs axially and this needs to be done in the future to investigate SC structure critically. On

top of that, expansion on mouse spermatocytes must be done in combination with denaturing at 95°C and increased NaCl concentration at 600 mM to test whether this can further increase signal ratio along the synaptonemal complex axis.

4.1. Complications and Recommendations

This series of experiments has shown promising results, but more research is needed. Much time was lost on optimising NHS ester dye pan staining because the stock solution of NHS ester dye was faultily dissolved. Because NHS esters are very reactive it is important to make sure that the solution is free of amino- and hydroxy-groups.

Due to the gelatinous consistency of hydrogels, handling them was precarious. Breaks and tears in hydrogels left many unusable pieces from the original samples. Handling of the hydrogel must be done very carefully with a small paintbrush as to not disturb it too much.

In this report Q is determined under the assumption of homogeneous hydrogel swelling. This assumption cannot be made with complete confidence without checking the true characteristics of hydrogel swelling. Just before completion of our experiments a pre-print method for quantitative ExM is offered [11]. GelMap introduces a fluorescent grid into pre-expanded hydrogels that scales with hydrogel swelling. With this method local deformations can be detected and accounted for. Furthermore, Q can be determined accurately in the x and y dimensions except for the z dimension. The grid offers the possibility of easily retrieving post-expansion cells and registering them in 3D to the pre-expansion of the same cell.

References

[1] *"ATTO NHS-Esters"*. "ATTO-TEC". Mar. 2021. URL: https://www.atto-tec.com/images/ATTO/Procedures/NHS.pdf.

[2] P. Castagnino & R. Assoian A. Cretu. "Studying the Effects of Matrix Stiffness on Cellular Function using Acrylamide-based Hydrogels". In: *Journal of Visualized Experiments* 42 (2010). The method for making siliconized slides was used from this paper. DOI: https://doi.org/10.3791/2089.

[3] G. Jenkins & I. Gwynn A.L. Barlow. "Scanning electron microscopy of synaptonemal complexes". In: *Chromosome Res* 1 (1993), pp. 9–13. DOI: https://doi.org/10.1007/BF00710602.

[4] E. Abbe. "Ueber einen neuen Beleuchtungsapparat am Mikroskop". In: *Archiv f. mikrosk. Anatomie* 9 (1873), pp. 469–480. DOI: https://doi.org/10.1007/BF02956177.

[5] Y. Zhao B.R. Gallagher. "Expansion microscopy: A powerful nanoscale imaging tool for neuroscientists". In: *Neurobiology of Disease* 154 (2021), p. 105362. ISSN: 0969-9961. DOI: https://doi.org/10.1016/j.nbd.2021.105362.

[6] Optical Imaging Center. *Leica SP8 STED*. 2023. URL: https://erasmusoic.nl/facility/equipment/leica-sp8-sted-be-311.

[7] N. Kleckner D. Zickler. "Pairing, and Synapsis of Homologs during Meiosis". In: *Cold Spring Harbor perspectives in biology* 7.6 (2015), a016626. ISSN: 0969-9961. DOI: https://doi.org/10.1101/cshperspect.a016626.

[8] R.R. Zhang & J.M. Gao F.G. Zhang. "The organization, regulation, and biological functions of the synaptonemal complex". In: *Asian Journal of Andrology Communications* 23.6 (2021), pp. 580–589. DOI: https://doi.org/10.4103/aja202153.

[9] M.C. Spindler et al. F.U. Zwettler. "Tracking down the molecular architecture of the synaptonemal complex by expansion microscopy". In: *Nature Communications* 11 (2020). DOI: https://doi.org/10.1038/s41467-020-17017-7.

[10] B. Mohar et al H.G.J. Damstra. "Visualizing cellular and tissue ultrastructure using Ten-fold Robust Expansion Microscopy (TREx)". In: *eLife* 1 (2022), e73775. DOI: https://doi.org/10.7554/eLife.73775.

[11] J.B. Passmore et al H.G.J. Damstra. "GelMap: Intrinsic calibration and deformation mapping for expansion microscopy". In: *bioRxiv* (2022). This article is a preprint and has not been certified by peer review. DOI: https://doi.org/10.1101/2022.12.21.521394.

[12] Z. Tong et al K. Xu. "Molecular organization of mammalian meiotic chromosome axis revealed by expansion STORM microscopy". In: *Proceedings of the National Academy of Sciences* 116.37 (2019), pp. 18423–18428. DOI: https://doi.org/10.1073/pnas.1902440116.

[13] J.A. Slotman et al L. Koornneef. "Multi-color dSTORM microscopy in Hormad1-/- spermatocytes reveals alterations in meiotic recombination intermediates and synaptonemal complex structure". In: *PLOS Genetics* 18.7 (2022), e1010046. DOI: https://doi.org/10.1371/journal.pgen.1010046.

[14] J. Bewersdorff O. M'Saad. "Light microscopy of proteins in their ultrastructural context". In: *Nature Communications* 11 (2020). DOI: https://doi.org/10.1038/s41467-020-17523-8.

[15] PLD. *Side reactions of N-hydroxysuccinimide esters with nucleophiles*. 2012. URL: https://chemistry.stackexchange.com/questions/423/side-reactions-of-n-hydroxysuccinimide-esters-with-nucleophiles.

[16] *Point-set registration*. 2023. URL: https://en.wikipedia.org/wiki/Point-set_registration.

[17] Polymerdatabase. *POLYACRYLATES*. 2022. URL: https://blog.polymerdatabase.com/polymer%5C%20classes/Polyacrylate%5C%20type.html.

[18] Polysciences. *Poly(acrylamide/acrylic acid) [60:40]*. 2023. URL: https://www.polysciences.com/india/polyacrylamideacrylic-acid-6040.

[19] M.I. Pigozzi & R. Benavente R.B. Sciurano. “Disassembly of the synaptonemal complex in chicken oocytes analyzed by super-resolution microscopy”. In: *Chromosoma* 128 (2019), pp. 443–451. DOI: https://doi.org/10.1007/s00412-019-00693-w.

[20] ThermoFisher Scientific. *Selection guide for endoplasmic reticulum stains*. 2022. URL: https://www.thermofisher.com/nl/en/home/life-science/cell-analysis/cell-structure/endoplasmic-reticulum.html#prd1.

[21] D.J. Wells. “Delineation of meiotic gene expression in male mice”. PhD thesis. University of Oxford, 2020.

[22] Youtube. *DJPC - Control expansion (DJPC mix)*. 2012. URL: https://www.youtube.com/watch?v=BPODHtRKTh4.

A

Computer Code

This appendix contains the code used during this experimental series.

A.1. Image Processing

This section shows the functions used to determine the number of fluorescent beads and their position in an image stack. This code was written in the ImageJ macro language

```
////////////////////////////////////////////////////////////////////////////////
begin = getTime();
title = getTitle();
selectWindow(title);
getVoxelSize(pw, ph, pd, unit);
getDimensions(width, height, channels, slices, frames);
setBatchMode(true);

////////////////////////////////////////////////
pw_array = newArray(1);
ph_array = newArray(1);
pd_array = newArray(1);
width_array = newArray(1);
height_array = newArray(1);
slices_array = newArray(1);

Array.fill(pw_array, pw*1e6);
Array.fill(ph_array, ph*1e6);
Array.fill(pd_array, pd*1e6);
Array.fill(width_array, width);
Array.fill(height_array, height);
Array.fill(slices_array, slices);
////////////////////////////////////////////////

maxtitle = "Max";//TitleMaker(title, "MAX", ".tif");

run("Z Project...", "projection=[Max Intensity]");
rename(maxtitle);

print("First directory is for max projection save location, second directory is for data
    sheets save location.");
directory1  = getDirectory("Select a Directory");
directory2  = getDirectory("Select a Directory");


selectWindow(maxtitle);
run("32-bit");
run("Gaussian Blur...", "sigma=2");

getStatistics(MAXarea, MAXmean, MAXmin, MAXmax, MAXstd, MAXhistogram);
prominence = MAXmean+MAXstd;

print("File: "+title);
```

```
print("PROMINENCE = "+prominence);

run("Find Maxima...", "prominence="+prominence+" output=[Point Selection]");
run("Set Measurements...", "center redirect=None decimal=3");
run("Measure");
selectWindow(maxtitle);
wait(4000);
close();


x = newArray(nResults);
y = newArray(nResults);


for (i=0; i<x.length; i++) {
        x[i]=getResult("XM", i);
        y[i]=getResult("YM", i);
}

z = Beads3D(x, y, title, pd);
x = Array.deleteValue(x, -1);
y = Array.deleteValue(y, -1);
z = Array.deleteValue(z, -1);
Table.reset("Results");
Table.setColumn("XM", x);
Table.setColumn("YM", y);
Table.setColumn("ZM", z);

tabletitle = title+"POINTS"+".csv";//TitleMaker(title, "POINTS", ".csv");
saveAs("Results", directory2+tabletitle);


nBeads = x.length;
print("BEADS = ", nBeads);
nBeads_array = newArray(1);
Array.fill(nBeads_array, nBeads);


Table.reset("Results");
Table.setColumn("pw", pw_array);
Table.setColumn("ph", ph_array);
Table.setColumn("pd", pd_array);
Table.setColumn("width", width_array);
Table.setColumn("height", height_array);
Table.setColumn("slices", slices_array);
Table.setColumn("nBeads", nBeads_array);
tabletitle = title+"DATA"+".csv";//TitleMaker(title, "DATA", ".csv");
saveAs("Results", directory2+tabletitle);
selectWindow(title);
close();
end = getTime();
print("RUNTIME = ", (end-begin)/1000, " seconds");


//This function returns the Zposition of all found beads and makes a 3D point in the z-stack
    of the image
function Beads3D(x, y, title, pd) {
        selectWindow(title);
        getDimensions(width, height, channels, slices, frames);
        z = newArray(x.length);


        //Loop over all found maxima
        for (i=0; i<x.length; i++) {

                if(i % (floor(x.length / 100)) == 0){
                        print( i / floor(x.length / 100));
                }


                makeRectangle(x[i]-5, y[i]-5, 10, 10);
```

```
                run("Plot Z-axis Profile");
                Plot.getValues(xpoints, ypoints);
                close();


                //Find the Z position with a gaussian fit to the profile
                Fit.doFit("Gaussian", xpoints, ypoints);
                z[i] = Fit.p(2);

                if (z[i] < 0){
                        x[i] = -1;
                        y[i] = -1;
                        z[i] = -1;}

                if (z[i] > slices) {
                        x[i] = -1;
                        y[i] = -1;
                        z[i] = -1;}
                }

        return z;
}


//Function which makes a standardised title for the image
function TitleMaker(string, whichfile, extension) {
        title = "";
        exornot = string.indexOf("EX");

        if (exornot == -1){
                expansion = "";
        }

        if (exornot != -1){
                expansion = " EX";
        }

        series = string.indexOf("zoutreeks") + 10;
        concentration = string.indexOf(".lif") + 7;

        title = whichfile+" "+string.substring(series, series+1)+expansion+" "+string.
            substring(concentration)+extension;

        return title;
}
```

A.2. Computational Model Hydrogel Swelling

This section shows the functions used to simulate fluorescent beads in a swelling hydrogel. This was written in Python This model was used to determine the accuracy in determination of Q based on the number of fluorescent beads sampled in the gel.

```
#%% IMPORTS
import numpy as np
import matplotlib.pyplot as plt
import time
import math as m
from mpl_toolkits import mplot3d
from scipy.spatial import distance
from scipy.optimize import curve_fit

#%% FUNCTIONs

def makePoints(xyzdim, nBeads, spread):
    """
    Makes N points in a selected volume defined by xyzdim spread homogeneuosly or randomly.
    Input: xyzdim as list, nBeads as int, spread as string.
    Output: numpy array with all points in the volume.
    """
    xdim = xyzdim[0]
```

```
    ydim = xyzdim[1]
    zdim = xyzdim[2]

    if spread == "random":
        return np.float32(np.random.rand(nBeads, 3) * [xdim, ydim, zdim])

    else:
        steps = m.floor(nBeads**(1/3))
        points = np.zeros((steps**3, 3))
        index = 0

        for i in range(steps):
            for j in range(steps):
                for k in range(steps):

                    points[index, 0] = (xdim / (steps)) * (i+0.5)
                    points[index, 1] = (ydim / (steps)) * (j+0.5)
                    points[index, 2] = (zdim / (steps)) * (k+0.5)
                    index += 1

        return points

def Expander(points, xyzPansion):
    """
    Transforms all points with expansion in x, y, and z
    Input: points as np array (matrix), Xpansions for xyz as float in list
    Output: transformed points as numpy array (matrix)
    """
    return np.multiply(points, xyzPansion)

def SelectPoints(points, x, y, z, width, height, depth):
    indices = np.where((points[:, 0] > x) & (points[:, 0] < (x + width))  &\
                       (points[:, 1] > y) & (points[:, 1] < (y + height)) &\
                       (points[:, 2] > z) & (points[:, 2] < (z + depth))  )

    return points[indices], indices

def getDistances(points, NN_index, indices):
    """
    Determines total, x, y, z, xy, xz, yz distance between two 3D coordinates.
    Input: two 3D coordinates as list
    Output: Distances as float in list
    """
    Distances = np.zeros((len(points), 7))
    x = points[:, 0]
    y = points[:, 1]
    z = points[:, 2]

    for i in range(len(x)):
        xdist2 = np.square(x[i] - x[int(NN_index[i])])
        ydist2 = np.square(y[i] - y[int(NN_index[i])])
        zdist2 = np.square(z[i] - z[int(NN_index[i])])

        Distances[i, 0] = np.sqrt(xdist2 + ydist2 + zdist2)
        Distances[i, 1] = np.sqrt(xdist2)
        Distances[i, 2] = np.sqrt(ydist2)
        Distances[i, 3] = np.sqrt(zdist2)
        Distances[i, 4] = np.sqrt(xdist2 + ydist2)
        Distances[i, 5] = np.sqrt(xdist2 + zdist2)
        Distances[i, 6] = np.sqrt(ydist2 + zdist2)

    meanDist = np.mean(Distances[indices], axis=0)

    return meanDist

def NaiveNN(points, x0, y0, z0, xdim, ydim, zdim):
    """
    Converts pixel coordinates to distance coordinates and determines the NN distance for
        eacht point in smaller volume set by a boundary based on concentration.
    Input: arrays with image data, matrix with all coordinates of beads.
    Output: points_mu, NN_index, BoundedIndices as lists.
```

```
    """
    # Load data
    nBeads = len(points)

    # Translate pixel points to distance points, calculate volume and which volume to take
        within the volume
    volume = np.product([xdim, ydim, zdim])
    border = 1.5*m.pow(volume / nBeads, 1/3)
    print('hallo', border, nBeads, xdim, ydim, zdim)
    border = 0


    # Determine which points are within the border
    indices = np.where((points[:, 0] > x0) & (points[:, 0] < (x0 + xdim - border)) &\
                       (points[:, 1] > y0) & (points[:, 1] < (y0 + ydim - border)) &\
                       (points[:, 2] > z0) & (points[:, 2] < (z0 + zdim - border)) )

    print('nogmaals', np.shape(points), np.shape(indices))

    # Calculate all distance for each point
    distances = distance.squareform(np.float32(distance.pdist(points)))
    distances[np.where(distances==0)] = np.sum(distances)

    NN_index = np.zeros(int(nBeads))
    NN_min = np.min(distances, axis = 0)

    # Determine minimum NN distance for eacht point and link point to other point
    for i in range(nBeads):
        NN_index[i] = np.where(distances[:, i] == NN_min[i])[0][0]

    return NN_index, indices

def NN_expansion(points, pointsEX, xyz0, xyz0EX, xyzdim, xyzdimEX):
    # Initalize variables
    x0 = xyz0[0]
    y0 = xyz0[1]
    z0 = xyz0[2]

    X0 = xyz0EX[0]
    Y0 = xyz0EX[1]
    Z0 = xyz0EX[2]

    xdim = xyzdim[0]
    ydim = xyzdim[1]
    zdim = xyzdim[2]

    xdimEX = xyzdimEX[0]
    ydimEX = xyzdimEX[1]
    zdimEX = xyzdimEX[2]

    NN_index, indices = NaiveNN(points, x0, y0, z0, xdim, ydim, zdim)
    meanDist = getDistances(points, NN_index, indices)

    NN_indEX, indicEX = NaiveNN(pointsEX, X0, Y0, Z0, xdimEX, ydimEX, zdimEX)
    meanDistEX = getDistances(pointsEX, NN_indEX, indicEX)


    EX = np.divide(meanDistEX, meanDist)

    return EX

def XYZ_NN_EX(points, pointsEX):
    #Initialize variables
    x = np.sort(points[:, 0])
    y = np.sort(points[:, 1])
    z = np.sort(points[:, 2])

    EX = np.sort(pointsEX[:, 0])
    EY = np.sort(pointsEX[:, 1])
    EZ = np.sort(pointsEX[:, 2])

```

```
159     NNxyz = np.zeros((len(points)-2, 3))
160     NNxyzEX = np.zeros((len(pointsEX)-2, 3))
161 
162     print(5, np.shape(pointsEX), np.shape(NNxyzEX), len(pointsEX))
163 
164     LoopLength = np.max([len(points), len(pointsEX)])
165 
166     for i in range(1, LoopLength - 1):
167 
168         if (i % 1e6) == 0:
169             print(i / 1e6)
170 
171         if i < (len(points) - 1):
172             NNxyz[i-1, 0] = np.min([abs(x[i] - x[i-1]), abs(x[i] - x[i+1])])
173             NNxyz[i-1, 1] = np.min([abs(y[i] - y[i-1]), abs(y[i] - y[i+1])])
174             NNxyz[i-1, 2] = np.min([abs(z[i] - z[i-1]), abs(z[i] - z[i+1])])
175 
176         if i < (len(pointsEX) - 1):
177             NNxyzEX[i-1, 0] = np.min([abs(EX[i] - EX[i-1]), abs(EX[i] - EX[i+1])])
178             NNxyzEX[i-1, 1] = np.min([abs(EY[i] - EY[i-1]), abs(EY[i] - EY[i+1])])
179             NNxyzEX[i-1, 2] = np.min([abs(EZ[i] - EZ[i-1]), abs(EZ[i] - EZ[i+1])])
180 
181     NNstats = np.zeros((2, 3))
182     NNstatsEX = np.zeros((2, 3))
183 
184     NNstats[0, :] = np.mean(NNxyz, axis=0)
185     NNstats[1, :] = np.std(NNxyz, axis=0)
186     NNstatsEX[0, :] = np.mean(NNxyzEX, axis=0)
187     NNstatsEX[1, :] = np.std(NNxyzEX, axis=0)
188 
189     return NNstats, NNstatsEX, NNxyz, NNxyzEX
190 
191 def RandomSampleCount(points, axis, xyzdim):
192     """
193     Creates a random sample of a volume within the total volume with points and counts the #
            points.
194     Input: points as np array (matrix), width, height, depth, xdim, ydim, zdim as float.
195     Output: Random Sample of points in a volume given by widht, height, depth in the
196             total volume xdim, ydim, zdim.
197     """
198     xdim, ydim, zdim = xyzdim[0], xyzdim[1], xyzdim[2]
199 
200     x = np.max([0, np.random.random() * xdim - axis])
201     y = np.max([0, np.random.random() * ydim - axis])
202     z = np.max([0, np.random.random() * zdim - axis])
203 
204     Sample_indices = np.where((points[:, 0] > x) & (points[:, 0] < (x + axis)) &\
205                               (points[:, 1] > y) & (points[:, 1] < (y + axis)) &\
206                               (points[:, 2] > z) & (points[:, 2] < (z + axis)) )
207 
208     nSampled = np.count_nonzero(Sample_indices)
209 
210     return nSampled
211 
212 def AccuracyVSnPoints(points, pointsEX, volperpoint, volperpointEX, \
213                       nSamples, expansion, iterations, xyzdim, xyzdimEX):
214     """
215     Determines the accuracy of Q based on #beads sampled for a number of times(iterations)
216     Input:  points & nSamples as np array, iterations as int, the rest as float
217     Output: The amount of beads in volume given as numpy arrays, vals and valsEX.
218     """
219 
220     vals = np.zeros((iterations, len(nSamples)))
221     valsEX = np.zeros((iterations, len(nSamples)))
222     axes = np.power(np.multiply(nSamples, volperpoint), (1/3))
223     EXes = np.power(np.multiply(nSamples, volperpointEX), (1/3))
224 
225     for i in range(len(nSamples)):
226         nSample = nSamples[i]
227 
228         print('loop 1', i)
```

```
229
230         for j in range(iterations):
231             print(nSample, axes[i], EXes[i])
232
233             nPoints_sample = RandomSampleCount(points, axes[i], xyzdim)
234             print(nPoints_sample)
235             vals[j, i] = nPoints_sample
236             nPoints_samplEX = RandomSampleCount(pointsEX, EXes[i], xyzdimEX)
237             print(nPoints_samplEX)
238             valsEX[j, i] = nPoints_samplEX
239
240             print('loop 2', j)
241
242     return vals, valsEX
243
244 #%% MAIN (NN distribution)
245 xyzdim = [18, 8, 0.170]
246 xyzPansion = [3, 20, 5]
247 xyzdimEX = np.multiply(xyzdim, xyzPansion)
248 print(xyzdimEX)
249 nPoints = int(1e8)
250 spread = "random"
251
252 points = np.load("points.npy")
253 pointsEX = np.float32(np.load("pointsEX.npy"))
254 NNxyz = np.float32(np.load("NNxyz.npy"))
255 NNxyzEX = np.float32(np.load("NNxyzEX.npy"))
256 fullstats = np.float32(np.load("fullstats.npy"))
257 fullstatsEX = np.float32(np.load("fullstatsEX.npy"))
258
259
260 width, height, depth = 0.1, 0.1, 0.1
261 widthEX, heightEX, depthEX = 0.4, 0.4, 0.4
262
263 SampledPoints, indices = SelectPoints(points, 2, 1, 0, width, height, depth)
264 SampledPointsEX = pointsEX[indices]
265 RandomSamplEX, randomIndices = SelectPoints(pointsEX, 2, 1, 0, widthEX, heightEX, depthEX)
266
267 NN_ex = NN_expansion(SampledPoints, SampledPointsEX, [2, 1, 0], [6, 20, 0], [0.1, 0.1, 0.1],
        [0.3, 2, 0.5])
268 xyzstats, xyzstatsEX, xyzNN, xyzNNEX = XYZ_NN_EX(SampledPoints, SampledPointsEX)
269 randstats, randstatsEX, randNN, randNNEX = XYZ_NN_EX(SampledPoints, RandomSamplEX)
270
271 print(np.divide(xyzstatsEX, xyzstats))
272 print(np.divide(randstatsEX, randstats))
273
274
275
276 #%% MAIN (Accuracy vs nBeads)
277 xyzdim = [20, 20, 10]
278 xyzPansion = [4.6, 4.6, 4.6]
279 xyzdimEX = np.multiply(xyzdim, xyzPansion)
280 nPoints = int(5e8)
281 spread = "random"
282
283 points = makePoints(xyzdim, nPoints, spread)
284 pointsEX = Expander(points, xyzPansion)
285
286
287 #%% Sampling Points
288
289 nSamples = (1e2, 2e2, 3e2, 4e2, 5e2, 6e2, 7e2, 8e2, 9e2, 1e3, 2e3, 3e3, 4e3, \
290             5e3, 6e3, 7e3, 8e3, 9e3, 1e4, 2e4, 3e4, 4e4, 5e4, 6e4, 7e4, 8e4, \
291             9e4, 1e5, 2e5, 3e5, 4e5, 5e5, 6e5, 7e5, 8e5, 9e5, 1e6)
292 volperpoint = m.prod(xyzdim) / nPoints
293 volperpointEX = m.prod(xyzdimEX) / nPoints
294 vols = np.multiply(nSamples, volperpoint)
295 volsEX = np.multiply(nSamples, volperpointEX)
296 iterations = 100
297 samplesfromiterations = 50
298
```

```
vals, valsEX = AccuracyVSnPoints(points, pointsEX, volperpoint, volperpointEX, \
                                 nSamples, xyzPansion[0], iterations, xyzdim, xyzdimEX)


Q = np.power(np.divide(np.multiply(vals, volsEX), np.multiply(valsEX, vols)), 1/3)
avgQ = np.average(Q, axis=0)
stdQ = np.std(Q, axis=0)
errorsQ = (abs(avgQ-4.6)/4.6*100)

#%% CURVE FIT AND PLOT FOR DETERMINATION OF ACCURACVY VS #BEADS
def linear(x, a, b):
    return a*x+b

def exponential(x, a, b):
    return a*x**b

x_data = np.log(np.array(nSamples))
y_data = np.log(np.array(stdQ))

popt, pcov = curve_fit(linear, x_data, y_data)
fit_lin = linear(x_data, popt[0], popt[1])

popt, pcov = curve_fit(exponential, np.array(nSamples), stdQ)
fit_exp = exponential(np.array(nSamples), popt[0], popt[1])


plt.plot(nSamples, stdQ, '.', label='simulated data')
a, b = str(round(popt[0], 3)), str(round(popt[1], 3))
fitlabel = f'$y={a}x^{b[0]}$'+f'$^{b[1]}$'+f'$^{b[2]}$'+f'$^{b[3]}$'+f'$^{b[4]}$'+f'$^{b[5]}$
    '
plt.plot(nSamples, fit_exp, label=fitlabel)
plt.legend(loc='upper right')
plt.yscale('log')
plt.xscale('log')
plt.grid()
plt.xlabel('$N_{beads}$')
plt.ylabel('$s_{Q}$')
```